Princeton Plasma Physics Laboratory

PPPL- 4581

PPPL- 4581

Development of a Spatially Resolving X-Ray Crystal Spectrometer For Measurement of Ion-temprature (Ti) And Rotation-velocity (v) Profiles in ITER

K. W. Hill, M. Bitter, L. Delgado-Aparicio, D. Johnson, R. Feder, P. Beiersdorfer, J. Dunn, K. Morris, E. Wang, M. Reinke, Y. Podpaly, J. E. Rice, R. Barnsley, M. O'Mullane, and S. G. Lee

December, 2010

PPPL
PRINCETON PLASMA PHYSICS LABORATORY

Prepared for the U.S. Department of Energy under Contract DE-AC02-09CH11466.

Princeton Plasma Physics Laboratory
Report Disclaimers

Full Legal Disclaimer

Trademark Disclaimer

PPPL Report Availability

Princeton Plasma Physics Laboratory:

http://www.pppl.gov/techreports.cfm

Office of Scientific and Technical Information (OSTI):

http://www.osti.gov/bridge

Related Links:

U.S. Department of Energy

Office of Scientific and Technical Information

Fusion Links

Development of a spatially resolving x-ray crystal spectrometer for measurement of ion-temperature (T_i) and rotation-velocity (v) profiles in ITER[a)]

K. W. Hill,[1,b)] M. Bitter,[1] L. Delgado-Aparicio,[1] D. Johnson,[1] R. Feder,[1] P. Beiersdorfer,[2] J. Dunn,[2] K. Morris,[2] E. Wang,[2] M. Reinke,[3] Y. Podpaly,[3] J. E. Rice,[3] R. Barnsley,[4] M. O'Mullane,[5] and S. G. Lee[6]
[1]*Princeton Plasma Physics Laboratory, P.O. Box 451 MS 15, Princeton, New Jersey 08543, USA*
[2]*Lawrence Livermore National Laboratory, Livermore, California 94550, USA*
[3]*MIT Plasma Science and Fusion Center, 190 Albany Street, Cambridge, Massachusetts 02139, USA*
[4]*ITER Cadarache JWS, Cadarache Centre, 13108 St Paul-Les-Durance, France*
[5]*Department of Physics, University of Strathclyde, Glasgow G4 0NG, United Kingdom*
[6]*National Fusion Research Institute, Daejeon 305-333, South Korea*

(Presented 19 May 2010; received 15 May 2010; accepted 27 August 2010; published online 26 October 2010)

Imaging x-ray crystal spectrometer (XCS) arrays are being developed as a US-ITER activity for Doppler measurement of T_i and v profiles of impurities (W, Kr, and Fe) with ~7 cm ($a/30$) and 10–100 ms resolution in ITER. The imaging XCS, modeled after a prototype instrument on Alcator C-Mod, uses a spherically bent crystal and 2D x-ray detectors to achieve high spectral resolving power ($E/dE > 6000$) horizontally and spatial imaging vertically. Two arrays will measure T_i and both poloidal and toroidal rotation velocity profiles. The measurement of many spatial chords permits tomographic inversion for the inference of local parameters. The instrument design, predictions of performance, and results from C-Mod are presented. © *2010 American Institute of Physics.* [doi:10.1063/1.3492414]

I. INTRODUCTION

A spatially resolving or 1D imaging x-ray crystal spectrometer (XCS) array is being designed to measure profiles of T_i, electron temperature (T_e), and plasma flow velocities on the International Tokamak Experimental Reactor (ITER).[1] This diagnostic is informed from prototype instruments already operating or to be installed on existing tokamaks throughout the world.[2,3] Favorable characteristics of this diagnostic are that it is very simple in structure, one instrument can measure the entire plasma profile, or a large fraction thereof, the spectrometer can continue taking data for long duration pulses, and it does not need neutral beam injection to operate. In this paper, we highlight the status of the instrument design and present some simulations of the expected temporal and spatial resolution of the measurements of T_i and v.

The imaging XCS diagnostic has been described in detail previously[2–5] and will only be briefly discussed here. It uses a spherically bent crystal to both disperse and image x rays emitted from the plasma onto a two-dimensional detector. This paper will focus on factors that will determine the expected performance of the ITER core imaging x-ray spectrometer.

II. MEASUREMENTS FROM ALCATOR C-MOD

To illustrate measurements from an imaging XCS, Fig. 1 shows data from the Alcator C-Mod tokamak. These are the uninverted or apparent T_i and the toroidal rotation velocity v as a function of time and vertical position at the central axis of the vacuum vessel for an H-mode discharge (No. 1080306014) with $I_p = 0.6$ MA, 1.6 MW of ion cyclotron range of frequencies (ICRF) rf heating from time 0.6 to 1.5 s, and an additional injection of 1 MW of lower hybrid (LH) rf with current-drive phasing between $t = 1.1$ and 1.36 s. During the Ohmic phase before $t = 0.6$ s, T_i is about 1.1 keV and v is about −15 km/s (counter to plasma current direction) in the plasma center. During the early part of the ICRF phase, after $t = 0.6$ s, T_i increases to 1.5 keV and v becomes positive at a value of 40 km/s in the core. After the LH injection begins, T_i increases further to 1.7 keV and the core velocity reduces until the LH turns off at 1.36 s, after which v begins to recover until the end of the ICRF heating phase. Discussions of the observed toroidal rotation velocity evolution with ICRF and LH heating have been published by Lin[6,7] and Ince-Cushman.[8] Of particular interest is the observation[7] that D(^{3}He) mode conversion ICRF generates core flow velocities about twice the magnitude of D(H) minority heating ICRF and the velocity profile is more centrally peaked, suggesting a mechanism for controlling the intrinsic rotation velocity profile.

The C-Mod spectrometer for He-like Ar measurements has a crystal-to-detector distance of 1.2 m and uses a quartz $(10\bar{1}2)$ crystal with dimensions of 2.7 cm × 6.4 cm bent to a

[a)]Contributed paper, published as part of the Proceedings of the 18th Topical Conference on High-Temperature Plasma Diagnostics, Wildwood, New Jersey, May 2010.
[b)]Author to whom correspondence should be addressed. Electronic mail: khill@pppl.gov.

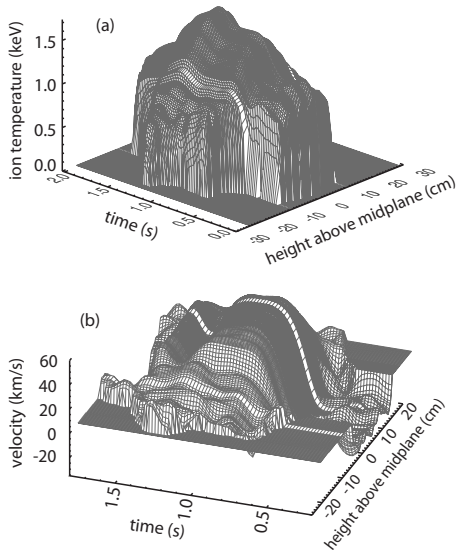

FIG. 1. (a) Ion temperature and (b) toroidal rotation velocity as a function of time and position above midplane (z) for plasma with ICRF plus LH rf injection.

radius of curvature of about 1.4 m. The Bragg angle is about 60°. The count rate in the He-like Ar resonance line for a 1 cm spatial resolution element passing through the plasma core in the discharge of Fig. 1 is about 1.5×10^6 counts/s, which provides measurements with 1% statistical error in 10 ms.

III. STATUS OF ITER SPECTROMETER DESIGN

The spectrometer will be housed inside the ITER equatorial port 9, as illustrated in Fig. 2. In order to measure x rays from the upper half of the ITER plasma cross section, two spherical crystals and associated arrays of imaging detectors will be used. This configuration will be replicated, with one spectrometer version viewing radially inward toward the tokamak center and the second instrument rotated ~10° about a vertical axis in order to view the plasma with an ~25% tangential component. The first spectrometer will measure T_i and poloidal flow velocities, and the second will measure T_i and toroidal flow velocities. The distance from crystal to detector will be about 1 m, only slightly smaller than the 1.2 m distance for the C-Mod spectrometer, and the chosen Bragg angle is about 43° in order to keep the detectors near the back of the ITER port plug for maximum neutron/gamma-ray shielding.

IV. SIMULATIONS OF PERFORMANCE

Several factors contribute to or affect the performance. First, the spectrometer must have sufficient wavelength resolution to effectively measure the small Doppler induced changes in line position and width from which the flow velocity and T_i are inferred. Second, the emission line must be sufficiently bright to enable enough photon counts to be collected from sufficiently small regions (chords) of the plasma in the desired time period, that is, the statistical uncertainties must be sufficiently small. Third, other factors that may degrade the measurement, such as instrumental or detector

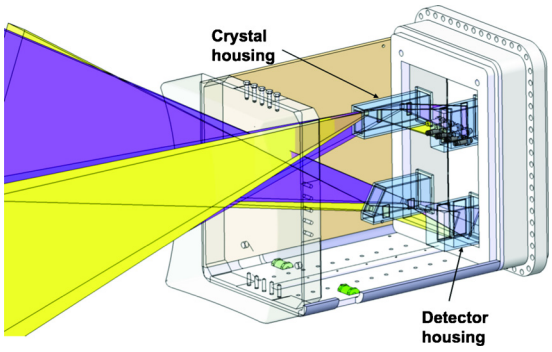

FIG. 2. (Color online) Illustration of crystals and detectors inside the individual secondary vacuum housings within the equatorial port plug 9. The ITER plasma is to the left.

variations in efficiency, background counts from nuclear radiation or x-ray continuum, or tomographic inversion effects, must be minimally perturbing.

A. Simulation of x-ray brightness

For the highest power phase of ITER operation, L-shell transitions of Ne-like W at x-ray energies near 8.3 and 9.1 keV have been identified as favorable for Doppler measurements.[1] Tungsten will be an indigenous impurity in ITER, as it is a component of the first wall and, thus, will not have to be artificially introduced into the plasma; the ionization potential of Ne-like W is sufficiently high that this charge state will exist over the electron-temperature (T_e) range of 10–30 keV; and the x-ray energies are in a region for which diffracting crystals with reasonably good reflectivity can be found.

Simulations of Ne-like W L-line brightness profiles were done, and an IDL code was developed to tomographically invert the "measured" brightnesses in order to infer the local emissivity T_i and v_{tor}. The SANCO impurity transport code was used to simulate the charge-state distribution and Ne-like W L-shell line emissivity for the ITER "scenario 2" H-mode plasma discharge.[9] Atomic data for the simulations were derived from ADAS.[10,11] This discharge has a centrally peaked T_e profile with a maximum value of 24 keV and a flat density profile with core density of 10^{20} electrons/cm^3. The W concentration was assumed to be 10^{-5} relative to the electron density. The peak emissivity of the 9.1 keV W L line is about 1.5×10^{11} photons cm^{-3} s^{-1}. An array of spectrometer sightlines was generated and the W line emissivity was integrated along the sightlines to simulate the line-brightness profile measured by the spectrometer. Then, the diffracted intensity of these lines from a crystal having an area of 25 cm^2 and an integrated reflectivity of 20 mrad was calculated to provide an estimate of the count rate from each spatial resolution element of the plasma.

The main parameter inferred from the simulation of line brightness and transmission through the spectrometer to the detector was a count rate per spatial resolution element versus radial position, which provides information on the statistical uncertainty of the values of T_i and v_{tor} that can inferred from the spectral lines. The ITER specifications call for measurement of T_i in 100 ms with 10% uncertainty and measure-

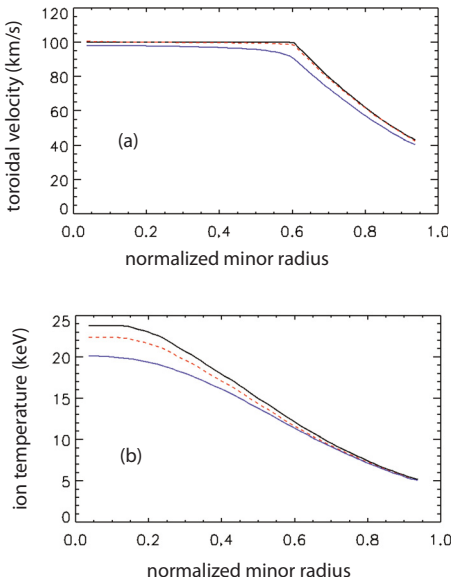

FIG. 3. (Color online) (a) Plasma toroidal flow velocity and (b) ion temperature vs normalized minor radius for ITER scenario 2 H-mode discharge. Curves shown are local values (upper solid) inferred from Gaussian fits to chordally integrated spectra (lower solid) and inverted from chordally integrated fits (dashed).

ment of v_{tor} in 10 ms with 30% uncertainty. For this simulation, a count rate for the central chord was 1.5×10^7 s^{-1}, and a count rate greater than 10^5 could be obtained for a viewing chord up to about 200 cm above the midplane or a normalized minor radius near 0.73. Thus, the statistical contributions to the uncertainty in T_i and v_{tor} would satisfy the ITER specifications up to this minor radius for the simulation conditions above. To make measurements further out in minor radius, lower Z ions, such as Fe, should be used.

B. Determination of T_i and v_{tor} from x-ray spectra

In addition, at each point along the sightlines, a Doppler shifted and broadened Gaussian line profile, weighted by the local emissivity, was generated at each point. For this simulation, the toroidal rotation velocity profile was chosen to be proportional to the T_e profile; the T_e profile was truncated at 10 keV and normalized to 100 km/s. This synthetic spectrum was integrated along each sightline to provide the spectral brightness, and this chordally integrated spectral line was fitted with a Gaussian function in order to infer the "apparent" or noninverted T_i and v_{tor} for that sightline. These apparent values are shown in Fig. 3 as the lower solid curves. The upper solid curves represent the local values. These comparisons show that the uninverted parameters inferred from the line-integrated spectra differ by less than 25% from the true local values.

C. Tomographic inversion of simulated spectra

The analysis of Condrea *et al.*[12] was used to perform a tomographic inversion of the simulated spectral brightnesses in order to reconstruct the local emissivity, T_i and v_{tor}. Concentric zones of constant poloidal flux were generated with flux values defined by those values at the points of tangency of the sightlines with the flux surfaces. Then, the L_{ij} matrix elements of Condrea *et al.* were calculated geometrically as the path lengths within zone i of the jth sightline, and the associated cos θ_{ij} values, where θ_{ij} is the angle between the jth line of sight and the local v_{tor} in zone i, were determined.

A comparison of the reconstructed local T_i and v_{tor} profiles with both the actual local values and the noninverted values is shown in Fig. 3 for the spectrometer that can measure a component of v_{tor}. We can see that the reconstruction of the v_{tor} profile is almost perfect, and the inverted T_i profile differs from the local values by less than 7%. For the strictly radially viewing spectrometer, the reconstructed central T_i is only 4% less than the local value. The discrepancy between the "local" T_i values along the sightlines and the reconstructed T_i values is believed to be partially due to the fact that the simulated "data" used for the inversion did not satisfy the assumptions of the inversion equations, namely, that the relevant plasma parameters (T_i and emissivity) were constant on flux surfaces. Work is in progress to replace the nonconstant values on each flux surface with the poloidal average value in order to see if the local T_i values can be reconstructed from the chordal averages by the inversion. Another possibility for the small discrepancy is that the actual profiles of the line-integrated spectra have a different shape than the fitted Gaussian line profiles that were used to infer the T_i values.

D. Effect of background noise on measurements

The detectors will have a uniformly distributed background count rate due to both x-ray continua diffracted from the crystal and noise counts due to the ambient fusion nuclear radiation that cannot be completely shielded out. An analysis of the contribution of this background to the uncertainty in measurement of T_i and v_{tor} has been presented previously. As an example, the uncertainty in the measurement of the line position, or v_{tor}, will be increased by a factor of 2 for a background level equal to the height of the spectral line. The uncertainty in measurement of the line width will be increased by a factor of 3 for this same background level. Thus, the uncertainty in T_i would be increased by a factor of 6 since $T_i \sim \sigma^2$, where σ is the width parameter of the spectral line's Gaussian distribution. Thus, an estimate of both the continuum backgrounds and a careful neutronics analysis need to be done in order to refine the present estimates of performance.

V. REDUCTION OF NUCLEAR RADIATION BACKGROUND BY PULSE HEIGHT DISCRIMINATION

Recent measurements on NSTX of the signals generated in a Pilatus II detector by the fusion neutrons and secondary gamma rays suggest that excellent discrimination against this nuclear background can be achieved by selection of a pulse-height window encompassing the narrow spectral band ($\Delta E/E \sim 0.01$) used to make the Doppler measurements. The detectors being used on the C-Mod imaging XCS are Pilatus 100 k sensors.[13] These devices are pixel array sensors having 487×195 individual x-ray photon counting detectors with size of 0.172×0.172 mm^2. Each pixel of the Pilatus II detector has only a single, lower level discriminator (LLD)

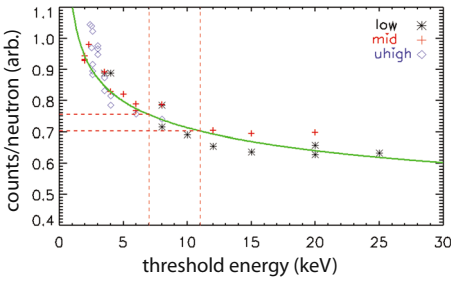

FIG. 4. (Color online) Counts in a Pilatus 100 k detector due to fusion nuclear radiation, normalized to the total number of NSTX neutrons, vs Pilatus energy threshold setting for low, mid-, and ultrahigh amplifier gain settings.

used for the rejection of electronic noise and fluorescence background. The total nuclear-radiation-generated background counts in all ~95 000 pixels of a Pilatus II detector were measured for different LLD settings ranging from 2 to 30 keV during several NSTX discharges. These data were then divided by the total number of neutrons generated during each discharge, and the resulting curve, as shown in Fig. 4, is normalized to 1 at the lowest possible threshold of ~2 keV; below 2 keV, the amplifier's electronic noise dominates the count rate.

The resulting curve approximates a power law with exponent −0.150 (solid curve in Fig. 4) and shows that a single LLD set to ~7 keV (for detection of 9 keV x rays) discriminates against only ~25% of the nuclear background. If, however, an additional upper level discriminator (ULD) set to ~11 keV is used, more than 90% of the nuclear background can be rejected. Since the width of the Pilatus pulse-height distribution is of the order of 500 eV full width at half maximum, this ~4 keV wide window should accept >95% of the x rays. Since, even with maximum nuclear shielding, the detector environment around ITER can be expected to have relatively high levels of nuclear radiation, it is important to encourage the pixel array detector developers to include both LLDs and ULDs in their electronics. The current Pilatus II detectors and the faster framing Eiger detectors[14] have only a single LLD. Each pixel of the Medipix II chip,[15] however, has both a LLD and a ULD, and would allow significant rejection of nuclear radiation background.

ACKNOWLEDGMENTS

This work was supported by the U.S. Department of Energy under Contract No. DE-ACO2-76-CHO-3073.

[1] P. Beiersdorfer, J. Clementson, J. Dunn, M. F. Gu, K. Morris, Y. Podpaly, E. Wang, M. Bitter, R. Feder, K. W. Hill, D. Johnson, and R. Barnsley, J. Phys. B **43**, 1 (2010).
[2] M. Bitter, K. W. Hill, A. L. Roquemore, P. Beiersdorfer, S. M. Kahn, S. R. Elliott, and B. Fraenkel, Rev. Sci. Instrum. **70**, 292 (1999).
[3] A. Ince-Cushman, J. E. Rice, M. Bitter, M. L. Reinke, K. W. Hill, M. F. Gu, E. Eikenberry, Ch. Broennimann, S. G. Lee, and Y. Podpaly, Rev. Sci. Instrum. **79**, 10E302 (2008).
[4] M. Bitter, K. W. Hill, B. Stratton, A. L. Roquemore, D. Mastrovito, S. G. Lee, J. G. Bak, M. K. Moon, U. W. Nam, G. Smith, J. E. Rice, P. Beiersdorfer, and B. S. Fraenkel, Rev. Sci. Instrum. **75**, 3660 (2004).
[5] K. W. Hill, M. L. Bitter, S. D. Scott, A. Ince-Cushman, M. Reinke, J. E. Rice, P. Beiersdorfer, M.-F. Gu, S. G. Lee, Ch. Broennimann, and E. F. Eikenberry, Rev. Sci. Instrum. **79**, 10E320 (2008).
[6] Y. Lin, J. E. Rice, S. J. Wukitch, M. J. Greenwald, A. E. Hubbard, A. Ince-Cushman, L. Lin, M. Porkolab, M. L. Reinke, and N. Tsujii, Phys. Rev. Lett. **101**, 235002 (2008).
[7] Y. Lin, J. E. Rice, S. J. Wukitch, M. J. Greenwald, A. E. Hubbard, A. Ince-Cushman, L. Lin, E. S. Marmar, M. Porkolab, M. L. Reinke, N. Tsujii, and J. C. Wright, Phys. Plasmas **16**, 056102 (2009).
[8] A. Ince-Cushman, J. E. Rice, M. Reinke, M. Greenwald, G. Wallace, R. Parker, C. Fiore, J. W. Hughes, P. Bonoli, S. Shiraiwa, A. Hubbard, S. Wolfe, I. H. Hutchinson, E. Marmar, M. Bitter, J. Wilson, and K. Hill, Phys. Rev. Lett. **102**, 035002 (2009).
[9] M. Shimada, ITER Report No. 27SZNW, 2004.
[10] H. P. Summers, The ADAS User Manual version 2.7, University of Strathclyde, Glasgow (2004), http://adas.phys.strath.ac.uk.
[11] H. P. Summers, W. J. Dickson, M. G. O'Mullane, N. R. Badnell, A. D. Whiteford, D. H. Brooks, J. Lang, S. D. Loch, and D. C. Griffin, Plasma Phys. Controlled Fusion **48**, 263 (2006).
[12] I. Condrea, E. Haddad, B. C. Gregory, and G. Abel, Phys. Plasmas **7**, 3641 (2000).
[13] Dectris Corp., http://www.dectris.com/sites/dectris.html.
[14] Paul Scherrer Institute, Villigen, Switzerland, http://pilatus.web.psi.ch/eiger.html.
[15] See http://medipix.web.cern.ch/MEDIPIX/ for information on Medipix 2 and Medipix 3 detector readout chips.

The Princeton Plasma Physics Laboratory is operated
by Princeton University under contract
with the U.S. Department of Energy.

Information Services
Princeton Plasma Physics Laboratory
P.O. Box 451
Princeton, NJ 08543

Phone: 609-243-2245
Fax: 609-243-2751
e-mail: pppl_info@pppl.gov
Internet Address: http://www.pppl.gov